Supporting Information

Mimicking the Nitric Oxide Dioxygenation (NOD) Reaction Cycle: A Comparative Study of "NOD Versus Dioxygen /or Nitric Oxide Activation"

Mahesh Yenuganti,[‖†] Sandip Das,[‖†] Kulbir,[‖†] Somnath Ghosh,[†] Prabhakar Bhardwaj,[†] Sonali Shivaji Pawar,[†] Subhas Chandra Sahoo[‡] Pankaj Kumar*[†]

[†]Department of Chemistry, Indian Institute of Science Education and Research (IISER), Tirupati 517507, India

[‡]Department of Chemistry, Punjab University, Punjab, Chandigarh, India

* To whom correspondence should be addressed.

E-mail: pankaj@iisertirupati.ac.in

Supporting Information S1

Table of Contents

Materials. All reagents and solvents obtained from commercial sources (Sigma Aldrich Chemical Co. and Tokyo Chemical Industry) were of the best available purity and used without further purification unless otherwise indicated. Solvents were dried according to reported literature and distilled under inert atmosphere before use.[S1] $H_2^{18}O_2$ (90.% ^{18}O-enriched) was purchased from ICON Services Inc. (Summit, NJ, USA). The 12-TMC ligand was prepared by reacting excess amounts of formaldehyde and formic acid with 1,4,7,10-tetraazacyclododecane as reported previously.[S2]

Instrumentation. UV-vis spectra were recorded on a Hewlett-Packard 8453 diode array spectrometer equipped with a thermostat cell holder (UNISOKU Scientific Instruments) designed for low-temperature experiments. FT-IR spectra in solid form were recorded on the Bruker-Alpha Eco-ATR FTIR spectrometer using the standard KBr disk method. ^{1}H-NMR spectra were measured with a Bruker model Ascend 400 FT-NMR spectrometer. Electrospray ionization mass spectra (ESI-MS) were recorded on an Agilent Mass Spectrometer (6200 series TOF/6500 series Q-TOF B.08.00), by infusing samples directly into the source using a manual method. The spray voltage was set at 4.2 kV and the capillary temperature at 80 °C. EPR spectral data were collected using an X-band Bruker EMX-plus spectrometer equipped with a dual-mode cavity at 100 K. The GC-MS analysis was recorded on an Agilent 7890B GC system equipped with a 5977B MSD Mass analyzer.

Nitric Oxide Preparation and Purification. Nitric oxide (NO) was prepared and purified by following a detailed procedure, as shown in Fig. S1. First, NO gas was prepared by the reaction of $NaNO_2$ with H_2SO_4 under an Argon (Ar) atmosphere and then passed through two different types of columns. Then NO gas passes through a column filled with NaOH beads to remove higher nitrogen oxides impurities. After that, the gas pass through a set of two columns filled with NaOH beads molecular sieves to remove the minor amount of remaining higher nitrogen oxides and moisture impurities. The highly purified NO gas was then collected

in a vacuum Schlenk flask fitted with a rubber septum (free from oxygen; after several cycles of vacuum and Ar purging). High pressure NO gas (with pressure >1 atmosphere; the septum bulges outward due to high pressures) then passed through an Ar saturated (oxygen-free) and dry Acetonitrile (CH_3CN) solution for 15 minutes. The concentration of NO in the NO saturated CH_3CN solution is ~14 mM.[S3]

Single-Crystal XRD Studies. The single crystals for **3**(NO_3)-(ClO_4) and **4**(NO_2)-(ClO_4) were obtained by slow diffusion of Et_2O into their CH_3CN solutions at -30 °C. Crystals were mounted on Hampton cryoloops. All geometric and intensity data for the crystals were collected using a Super-Nova (Mo) X-ray diffractometer equipped with a micro-focus sealed X-ray tube Mo-Kα ($\lambda = 0.71073$ Å) X-ray source and HyPix3000 (CCD plate) detector of with increasing ω (width of 0.3 per frame) at a scan speed of either 5 or 10 s/frame. The CrysAlisPro software was used for data acquisition and data extraction. Using Olex2[S4], the structure was solved with the SIR2004[S5] structure solution program using Direct Methods and refined with the ShelXL[S6] refinement package using Least Squares minimization. All non-hydrogen atoms were refined with anisotropic thermal parameters. Few anions mainly ClO_4 ions were found to be highly disordered, and appropriate disordered model applied (Figure S16 and S17). Detail crystallographic data and structural refinement parameters are summarized in Table T1 – T2. CCDC 1997187 (**3**) and 1997186 (**4**), contains the supplementary crystallographic data for this paper. Crystallographic data can be obtained free of charge from the Cambridge Crystallographic Data Centre (CCDC) via www.ccdc.cam.ac.uk/data_request/cif (or from the Cambridge Crystallographic Data Centre, 12, Union Road, Cambridge CB2 1EZ, UK; fax: (+44) 1223-336-033; or deposit@ccdc.cam.ac.uk).

Reactivity Studies. All UV-vis spectral measurements were run in a UV cuvette in CH_3CN solutions under Ar at different tempratures. All kinetic reactions were run at least three times, and the data reported here are the average outcome for these reactions. We have performed all

the reactions in the degassed solutions under Ar to avoid the interaction/reaction of dioxygen with nitric oxide. Formation of complexes **3** and **4**, in the NOD reactions of **1** and **2** (respectively), were identified by comparing with the authentic samples, and product yields were determined by comparison against standard curves prepared with authentic samples.[S7-S10]

FT-IR Spectroscopy and ^{18}O-labeling Experiments. We have recorded the FT-IR spectra of different complexes in their solid form as KBr pellets to follow the source of oxygen in the NOD products. All the spectra were recorded for the isolated products after the completion of the reaction at RT. The IR spectra of **3** showed a characteristic peak at 1385 cm^{-1} for nitrate (^{14}N^{16}O$_3^-$), which shifted to 1335 cm^{-1} when prepared in the reaction of **1**-(^{18}O$_2^{2-}$) with ^{14}NO. The change in the IR stretching frequency of nickel bound nitrate ($\Delta = 50$ cm^{-1}) confirmed clearly that the increase in the reduced mass of oxygen atom (^{16}O to ^{18}O) by four amu is responsible for the decrease in the stretching frequency of nitrate (**3**-(^{18}O$_2$N^{16}O$^-$)) functional group (SI, Figure S2). We observed the similar spectral changes when the IR spectra of the NOD reaction product of **2**-(^{16}O$_2^{2-}$). The IR spectra of complex **4**-(^{16}ON^{16}O) showed a characteristic nitrite stretching frequency at 1271 cm^{-1}, which shifted to 1240 cm^{-1} (^{18}ON^{16}O$^-$) when O$_2^{2-}$ moiety of **2** was prepared with ^{18}O-labeled H$_2$^{18}O$_2$ (SI, Figure S7).

NOD Reaction and ^{18}O-labeling Experiments by ESI-Mass Spectrometry. We have recorded the ESI mass spectra for the NOD products, after completion of the reaction, in CH$_3$CN and at RT. To identify and establish the source of oxygen, complexes **1** and **2** having ^{18}O-labeled O$_2^{2-}$ moiety ([[(12-TMC)Nio^{III}(^{18}O$_2^{2-}$)]$^+$ and ([(12-TMC)Co^{III}(^{18}O$_2^{2-}$)]$^+$), were reacted with one fold NO in CH$_3$CN under Ar at 233 K. For this experiment, two different schlenk tube (25 mL) equipped with CH$_3$CN solution of **1** and **2** (0.5 mM / 10 mL) sealed with a rubber septum was reacted with one fold NO under an Ar atmosphere. The reaction mixtures were kept for one hour, and then ESI mass spectra of the solutions in CH$_3$CN were recorded.

Detection of Peroxynitrite intermediate (•NO₂ radical trapping experiment). To confirm the formation of Ni^{II}-PN, we have performed the phenol ring nitration test by trapping •NO₂ (formed by the homolysis of ONO-O⁻ moiety of M-PN intermediate) using 2,4-di-*tert*-butyl phenol (2,4-DTBP). In this regard, first, we have reacted **1** (1.0 mM) with one equivalent of NO in the presence of 2,4-DTBP (5.0 mM) in CH₃CN at 233 K under Ar. The reaction mixture was kept for one hour at RT and then analyzed by GC-MS and HPLC for qualitative and quantitative estimation against the standard plots of various compounds. In this experiment, we have observed the formation of NO₂-2,4-DTBP with 2,4-DTBP-D (SI, Figure S14), suggesting the formation of Ni^{II}-PN intermediate and homolysis of O-ONO⁻ moiety to form •NO₂, which is responsible for the formation of various products from 2,4-DTBP. The amount of NO₂-2,4-DTBP formed in the reaction was found to be ~ 60 ($\pm$ 2)% and ~ 10 ($\pm$ 2) % 2,4-DTBP-D in the reaction mixture, because a small amount of Ni^{II}-PN decomposes to Ni^{II}-NO₃⁻ due to the isomerization of ONOO⁻ to NO₃⁻. Also, we have identified the formation of proposed Co^{II}-PN intermediate by phenol ring nitration test using 2,4-DTBP. In this trapping experiment also, we had observed the formation of PN driven products (NO₂-2,4-DTBP and 2,4-DTBP-D) when **2** was reacted with one fold NO in the presence of 2,4-DTBP. In this regard, we have reacted **2** (1.0 mM) with NO (1.0 mM) in the presence of 2,4-DTBP (5.0 mM) in CH₃CN at 258 K under Ar. The reaction mixture was then kept for one hour at RT and then analyzed and quantified by GC-MS and HPLC against the standard plots of all the compounds. In this reaction, we observed the formation of the NO₂-2,4-DTBP {~ 45 ($\pm$ 2) %} and dimerized product, 2,4-DTBP-D, {~ 15 ($\pm$ 2)%} product mixture. As known from the literature, PN reaction with 2,4-DTBP generates the NO₂-2,4-DTBP and hence confirm the putative PN intermediate formation in the reaction of both the complexes (**1** & **2**) with NO.

Control Experiments on 2,4-DTBP: In order to confirm the proposed [Ni-PN]$^{+}$ intermediate, in the NOD reaction of 1, we have explored the phenol ring nitrosation in various

experimental conditions. As already confirmed, *indirectly, a metal-PN has been well characterized/explored by **PHENOL-RING-NITROSASTION TEST** using 2,4-DTBP (wide supra), and a vast literature is available on the same chemistry. In case of NOD reaction of 1, UV-Visible spectral evidence showed a new band, proposed to be Ni^{2+}-PN, before the generation of $Ni^{2+}NO_3^-$.. Furthermore, to support our assumption, we have performed/included the following control experiments*

*(**a**) Added 2,4,-DTBP (5.0 mM) after the completion of NOD reaction of **1** (1.0 mM).*

*(**b**) **1** (1.0 mM) + 2,4,-DTBP (5.0 mM) without addition of NO*

*(**c**) 2,4,-DTBP (5.0 mM) + NO*

*In these experiments (a, b & c), we did not observe the ring-nitration product (NO_2-2,4-DTBP), supporting our proposition Ni-PN intermediate in the NOD reaction of complex **1**. The product analysis using GC only showed the 2-4-DTBP and a very small amount of 2,4-DTBP-D (0.5 to 1 %) in case of experiment b. While in experiment a and c, we only observed 2,4-DTBP, no NO_2-2,4-DTBP in any of these control experiments.*

Qualitative and quantitative estimation of NO_2^- and NO_3^- by Griess reagent test. Griess reagent test was performed for qualitative and quantitative estimation of NO_3^- and NO_2^- in the reaction of **1** and **2** with one fold NO, respectively. Griess reagent is known to detect and analyze the NO_2^- ion by the formation of an azo dye (red-pink color). But, it is not active towards NO_3^- ions; however, upon addition of VCl_3 to Griess reagent (modified Griess reagent), it shows the formation of azo dye (red-pink color). Therefore, Greiss reagent can easily distinguish between NO_2^- and NO_2^- and can also be quantified following the UV-vis calibration plot.

Nitrate estimation by modified Griess reagent. Complex **1** (0.5 mM, 10 mL) was reacted with one equivalent of NO under the Ar atmosphere at $-40 °C$. The color of the solution was changed from green to light blue. After the completion of the reaction, the reaction mixture

was kept at room temperature for about 30 minutes and then dried on the rotary evaporator. We have added water (5.0 mL) to the dried product, and then a solution of Na_2S (5.0 mM, 5.0 mL) was added, and the reaction mixture was kept for 30 minutes. Nickel precipitates as NiS and separated by filtration. The organic component of the reaction mixture was separated from the aqueous layer using $CHCl_3$. We have diluted the aqueous layer up to 10 mL. To prepare the sample for quantification of NO_3^-, 25 µL of this solution was added to a sample vial containing 1.0 mL of freshly prepared modified Griess reagent and then diluted to 2.5 mL by adding H_2O. The modified Griess reagent was prepared by mixing sulphanilic acid (0.2%), naphthylethylenediamine dihydrochloride (0.01%), and VCl_3 (0.8 % in 1M HCl) in aqueous solution. We did not observe any color change immediately, but after keeping for overnight, the color of the solution was changed to violate-pink. We have compared the UV-vis spectra of this solution with a calibration plot prepared by employing authentic $NaNO_3$ solutions (SI, Figure S13). The yields of nitrate determined by using modified Griess reagent in the reaction of 1 with NO was 85 ± 4 %.

To obtain the calibration curve, the stock solutions of $NaNO_3$ in various concentration (0, 0.20, 0.40, 0.60, 0.80, 1.00, 1.20, 1.40, 1.60, 1.80, 2.00 mM) were prepared and 25 µL of each stock solution was added to a sample vial containing 1.0 mL of fresh prepared modified Griess reagent and then diluted to 2.5 mL by adding H_2O. We recoded UV-vis spectra for each standard solution and a calibration plot was prepared with varying concentrations of nitrate (0, 2.0, 4.0, 6.0, 8.0, 10, 12, 14, 16, 18, 20 µM) and corresponding λ_{max} at 547 nm (SI, Figure S13b).

Nitrite estimation by Griess reagent. The amount of NO_2^- formed in the reaction of **2** (0.5 mM) and NO was determined by using Griess reagent and following the same procedure as explained for NO_3^- (vide supra). The Griess reagent was prepared by mixing sulphanilic acid (2.0%), naphthyl ethylenediamine dihydrochloride (0.2%) in aqueous phosphoric acid (5.0%).

We observed the immediate color change as 25 μL of the extracted aqueous solution (10 mL) was added to a sample vial containing 1.0 mL of Griess reagent. We have compared the UV-vis spectra of this solution with a calibration plot prepared by employing authentic $NaNO_2$ solutions (SI, Figure S13). The yields of nitrite determined by using Griess reagent in the reaction of **1** with NO was 90 ± 2 %.

To obtain the calibration curve, the stock solutions of $NaNO_2$ in various concentration (0, 0.25, 0.50, 0.75, 1.00, 1.25, 1.50, 1.75, 2.00, 2.25, 2.50 mM) were prepared and 25 μL of each stock solution was added to a sample vial containing 1.0 mL of fresh prepared Griess reagent and then diluted to 2.5 mL by adding H_2O. We recorded UV-vis spectra for each standard solution and a calibration plot was prepared with varying concentrations of nitrite (0, 2.5, 5.0, 7.5, 10, 12.5, 15, 17.5, 20, 22.5, 25 μM) and corresponding λ_{max} at 547 nm (SI, Figure S13b).

NOD reaction 1 {Formation of $[(12\text{-TMC})Ni^{II}(NO_3^-)]^+$ $(3\text{-}NO_3^-)$}. Complex **1** was reacted with an equimolar amount of NO in CH_3CN under Ar to determine the product of the NOD reaction. To confirm the NOD reaction product, complex **1** (84 mg, 0.2 mmol) was reacted with one equivalent of NO in CH_3CN at 233 K under an Ar atmosphere. Upon reaction with NO, the color of the reaction mixture changes from light green to light blue, indicating the formation of a new product (**3**). The reaction mixture further stirred for 30 minutes at 273 K under the Ar atmosphere. Excess diethyl ether was added to yield light blue powder, which was collected by filtration and further washed with diethyl ether and dried under vacuum. Further the blue powder was dissolved in ACN and layered with diethyl ether to obtain a good deep blue colored crystal. Yield: 85 mg (95 %). UV: $\lambda_{max} = 370$ nm. FT-IR (KBr pellet): 2925, 1385, 1089 cm^{-1}. Mass (*m/z*): Calcd*:* 348.1, Found: 348.1. Anal. Calcd. For $C_{12}H_{28}ClN_5NiO_7$: C, 32.13; H, 6.29; N, 15.61; Found : C, 32.28; H, 6.31; N, 15.56. ^1H NMR (CD_3CN): ~113 (6H, -CH_3), ~124 (6H, -CH_3), ~133 (8H, -CH_2), ~142 (8H, -CH_2). X-ray crystallography suitable crystals were obtained by vapor diffusion of Et_2O to a CH_3CN solution of **3** at 253 K.

NOD reaction 2 {Formation of [(12-TMC)Co^{II}(NO$_2^-$)]$^+$ (4-NO$_2^-$)}. The addition of NO to a solution of **2** resulted in the generation of **4**. The characteristic UV-Vis absorption bands of **2** (λ_{max} = 350 nm and 560 nm) changed to a new band (λ_{max} = 535 nm), which corresponds to **4**, within 50 minutes in CH$_3$CN at 233 K under an Ar atmosphere. Further, for various spectral characterization, we have isolated the end product (**4**) of the reaction of **2** with an equimolar amount of NO under the given reaction conditions. Complex **2** (85 mg, 0.2 mmol) reacted with an equimolar amount of NO at 253 K in CH$_3$CN under the Ar atmosphere. The color of the reaction mixture changes from purple to light pink within 20 minutes upon the addition of NO. The reaction mixture further stirred for an additional 30 minutes at 253 K and then warmed to RT and stirred for an additional 30 minutes under Ar atmosphere. The complex was dried under vacuum and washed with diethyl ether several times and again dried under vacuum to afford light pink powder. The FT-IR spectrum of **4** showed a characteristic peak for Co^{II}-bound NO$_2^-$ at 1271 cm^{-1}, which shifted to 1240 cm^{-1} when exchanged with ^{18}O-labeled-**2**, i.e., [(12TMC)Co^{III}(^{18}O$_2^{2-}$)]$^+$ (Figure S12). The ESI-MS spectrum of the **4** exhibited a prominent peak at m/z 333.16, [(12TMC)Co^{II}(N^{16}O$_2^-$)]$^+$ (calcd m/z 333.16). However, this peak shifted to m/z 335.16, [(12TMC)Co^{II}(^{18}ON^{16}O$^-$)]$^+$ (calcd m/z 335.16) (Figure S13) when the reaction was performed with ^{18}O-labeled **2**, i.e., [(12TMC)Co^{III}(^{18}O$_2^{2-}$)]$^+$; demonstrating clearly that the nitrite (^{16}ON^{18}O$^-$) ligand in **4** is derived from O$_2^{2-}$ moiety of **2**.. Yield: 75 mg (85 %). UV: λ_{max} = 535 nm (ε = 24 M^{-1} cm^{-1}). FT-IR (KBr pellet): 2925, 1271, 1084, 755 cm^{-1}. Mass (*m/z*): Calcd*:* 333.1, Found: 333.1. Crystals suitable for X-ray crystallography were obtained on keeping the acetonitrile solution of **4** layered with diethyl ether at 253 K for several days.

Synthesis of [(12-TMC)Co^{II}(NO$_2^-$)](ClO$_4$). To a 20 ml CH$_3$CN solution of [(12-TMC)Co^{II}(CH$_3$CN)](ClO$_4$)$_2$ (502 mg, 1 mmol), 0.3 mL aqueous solution of NaNO$_2$ (69 mg, 1 mmol) was added slowly with constant stirring. The color of the reaction mixture changed from wine red to light pink over 5 min after the addition of NaNO$_2$.The mixture was stirred for one

hour at RT. The volume of the reaction mixture was then decreased to 10 mL over a rotary vacuum and then layered with diethyl ether and kept for crystallization at 253 K. Yield: 400 mg (~ 95 %). UV: λ_{max} = 535 nm (ε = 24 M^{-1} cm^{-1}). FT-IR (KBr pellet): 2925, 1271, 1089, 755 cm^{-1}. Mass (m/z): Calcd: 333.1, Found: 333.1.

Magnetic moment calculation and determination of number of unpaired electrons in complex 3: Evans' method of ^{1}H-NMR was performed to determine the number of unpaired electrons (spin state) in complex **3** at room temperature[S11-S13]. A WILMAD® coaxial insert (with a sealed capillary) tube containing the only CD$_3$CN solvent (with 1.0% TMS) was inserted into the normal NMR tubes containing the complex **3** (4.0 mM, with 0.1% TMS). We have calculated the chemical shift value of the TMS peak in the presence of the complex **3** with respect to that of the TMS peak in the outer NMR tube. The magnetic moment was calculated using the given equation,

$$\mu_{eff} = 0.0618(\Delta vT / 2fM)^{1/2}$$

$$\mu_{eff} = 0.0618 * (26.76 * 298 / 2 * 400 * 0.004)^{1/2}$$

$$\mu_{eff} = 3.08 \text{ BM}$$

Where f = oscillator frequency (MHz) of the superconducting spectrometer, T = absolute temperature, M = molar concentration of the complex **3**, and v = difference in frequency (Hz) between the two TMS signals[S13]. The calculated magnetic moment of complex **3** was determined to be 3.08 BM in CD$_3$CN at RT, suggesting 2 unpaired electrons in Ni^{2+} centre of complex **3**.

References

S1. Armarego, W. L. F.; Chai, C. L. L. *Purification of Laboratory Chemicals*, 6th ed.; Pergamon Press: Oxford, **2009**.

S2. Puthiyaveetil Yoosaf, M. A.; Ghosh, S.; Narayan, Y.; Yadav, M.; Sahoo, S. C.; Kumar, P., Finding a new pathway for acid-induced nitrite reduction reaction: formation of nitric oxide with hydrogen peroxide. *Dalton Transactions* **2019**, *48*, 13916-13920.

S3. Young, C. L. *Solubility Data Series Val. 8 Oxides of Nitrogen,* International Union of Pure and Applied Chemistry (IUPAC), 1981.

S4. Dolomanov, O. V.; Bourhis, L. J.; Gildea, R. J.; Howard, J. A. K.; Puschmann, H. OLEX2: a Complete Structure Solution, Refinement and Analysis Program. *J. Appl. Cryst*. **2009**, *42*, 339–341.

S5. Burla, M. C.; Caliandro, R.; Camalli, M. C., B.; Cascarano, G. L.; De Caro, L.; Giacovazzo, C.; Polidori, G.; Siliqi, D.; Spagna, R. IL MILIONE: A Suite of Computer Programs for Crystal Structure Solution of Proteins. *J. Appl. Cryst.* **2007**, *40*, 609–613.

S6. G. M. Sheldrick. Crystal Structure Refinement with SHELXL. *Acta Cryst*. **2015**, *C71*, 3–8.

S7. Cho, J.; Sarangi, R.; Kang, H. Y.; Lee, J. Y.; Kubo, M.; Ogura, T.; Solomon, E. I.; Nam, W., Synthesis, structural, and spectroscopic characterization and reactivities of mononuclear cobalt(III)-peroxo complexes. *J. Am. Chem. Soc.* **2010,** *132* (47), 16977-86.

S8. Cho, J.; Sarangi, R.; Annaraj, J.; Kim, S. Y.; Kubo, M.; Ogura, T.; Solomon, E. I.; Nam, W., Geometric and electronic structure and reactivity of a mononuclear 'side-on' nickel(iii)–peroxo complex. *Nature Chem.* **2009,** *1* (7), 568-572.

S9. Kumar, P.; Lee, Y. M.; Park, Y. J.; Siegler, M. A.; Karlin, K. D.; Nam, W., Reactions of Co(III)-nitrosyl complexes with superoxide and their mechanistic insights. *J Am Chem Soc* **2015,** *137* (13), 4284-7.

S10. Puthiyaveetil Yoosaf, M. A.; Ghosh, S.; Narayan, Y.; Yadav, M.; Sahoo, S. C.; Kumar, P., Finding a new pathway for acid-induced nitrite reduction reaction: formation of nitric oxide with hydrogen peroxide. *Dalton Trans.* **2019,** *48* (37), 13916-13920.

S11. Evans, D. F. The determination of the paramagnetic susceptibility of substances in

solution by nuclear magnetic resonance. J. Chem. Soc. 2003-2005 (1959).

S12. Lölinger, J. & Scheffold, R. Paramagnetic moment measurements by nmr. A micro technique. J. Chem. Edu. 646-647 (1972).

S13. Evans, D. F. & Jakubovic, D. A. Water-soluble hexadentate Schiff-base ligands as sequestrating agents for iron(III) and gallium(III). J. Chem. Soc. Dalton Trans. 2927-2933 (1988).

Table T1 Crystallographic data for **3** and **4**.

	3	**4**
Chemical formula	$C_{12}H_{28}ClN_5NiO_7$	C12H28ClCoN5O6
Formula weight	450.55	432.77
Wavelength /Å	0.71073	0.71073
Crystal system	orthorhombic	monoclinic
Space group	Pnma	$P2_1$
T, K	293(2)	293(2)
a, Å	13.8307(4)	8.1078(2)
b, Å	9.6928(2)	15.0999(3)
c, Å	14.1541(4)	8.1316(2)
α, °	90	90
β, °	90	110.722(2)
γ, °	90	90
V/ Å^3	1897.47(9)	931.12(4)
Z	4	2
Calculated density, g/cm^3	1.570	1.544
Abs. Coeff. /mm^{-1}	1.208	1.103
Reflections collected	9087	11321
Unique reflections	2154	3659
Refinement method	Least-squares on F^2	Least-squares on F^2
Data/restraints/parameters	2154/0/156	3659/1/225
Goodness-of-fit on F^2	1.035	1.126
Final R indices [$I > 2\sigma(I)$]	R1 = 0.0408	R1 = 0.0777
	wR2 = 0.1086	wR2 = 0.1820
R indices (all data)	R1 = 0.0485	R1 = 0.0791
	wR2 = 0.1147	wR2 = 0.1827

Table T2 Selected bond lengths (Å) and bond angles (°) for **3** and **4**.

	3		**4**
Ni1 O1	2.1521(19)	Co1 O2	2.17(1)
Ni1 O1	2.1521(19)	Co1 O1	2.15(1)
Ni1 N2	2.083(2)	Co1 N2	2.20(1)
Ni1 N1	2.125(3)	Co1 N3	2.145(9)
Ni1 N3	2.129(3)	Co1 N1	2.161(9)
Ni1 N2	2.083(2)	Co1 N4	2.20(1)
O1 Ni1 O1	59.37(10)	O2 Co1 N1	133.6(4)
N2 Ni1 O1	154.75(8)	O2 Co1 N2	93.5(4)
N2 Ni1 O1	95.38(8)	O2 Co1 N3	90.3(4)
N2 Ni1 O1	95.38(8)	O2 Co1 N4	128.5(4)
N2 Ni1 O1	154.75(8)	O2 Co1 O1	57.4(4)
N2 Ni1 N2	109.86(12)	N1 Co1 N2	80.8(4)
N2 Ni1 N1	84.68(7)	N1 Co1 N3	133.2(4)
N1 Ni1 O1	98.47(9)	N1 Co1 N4	81.1(4)
N1 Ni1 O1	98.47(9)	N1 Co1 O1	92.5(4)
N1 Ni1 N3	161.02(11)	N2 Co1 N3	81.5(4)
N3 Ni1 O1	98.00(9)	N2 Co1 N4	134.3(4)
N3 Ni1 O1	98.00(9)	N2 Co1 O1	131.1(4)
N2 Ni1 N1	84.68(7)	N3 Co1 N4	81.1(4)
N2 Ni1 N3	84.45(7)	N3 Co1 O1	130.7(4)
N2 Ni1 N3	84.45(7)	N4 Co1 O1	91.2(4)
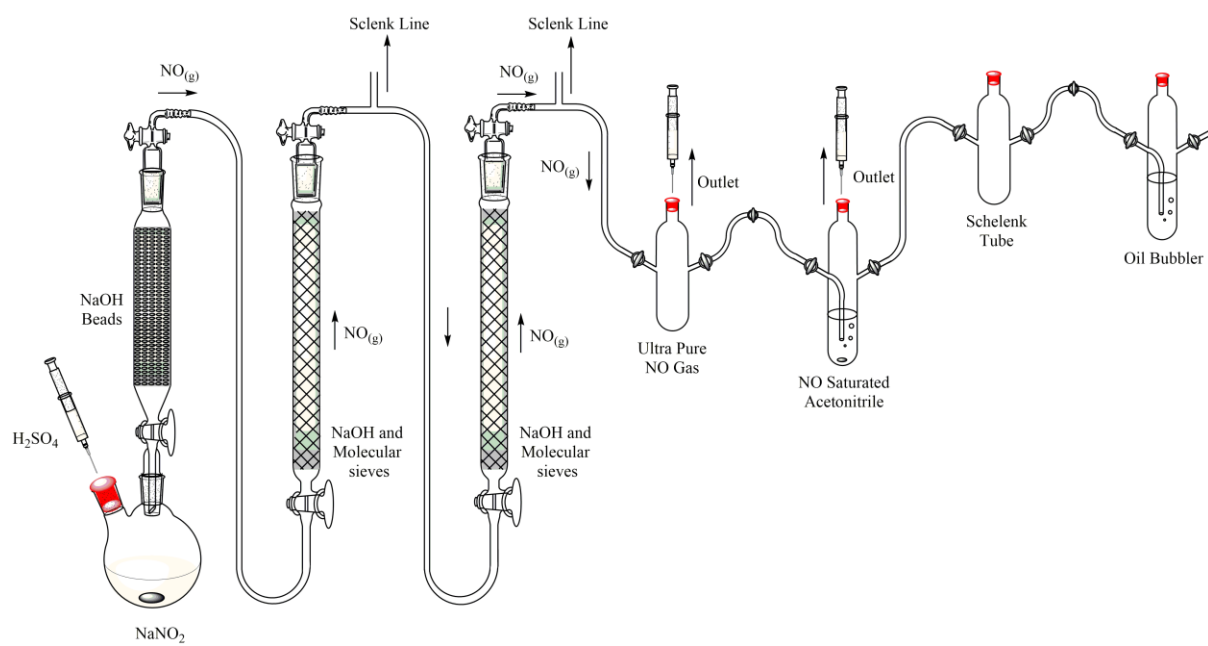
Figure S1. Schematic diagram showing the generation and purification setup for NO.
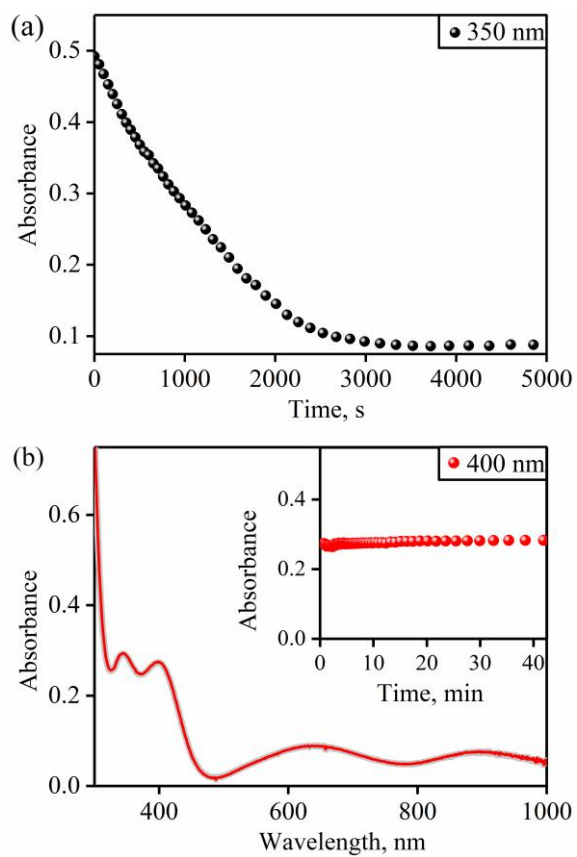
Figure S2. (a) Time course of decomposition of intermediate in the reaction of **1** (1 mM) with NO (black circles) monitored at 350 nm in CH$_3$CN at 233 K. (b) UV-vis spectra for the natural decay of **1**. The Inset shows the time course of the natural decay of **1** (red circles) monitored at 400 nm in CH$_3$CN at 233 K.
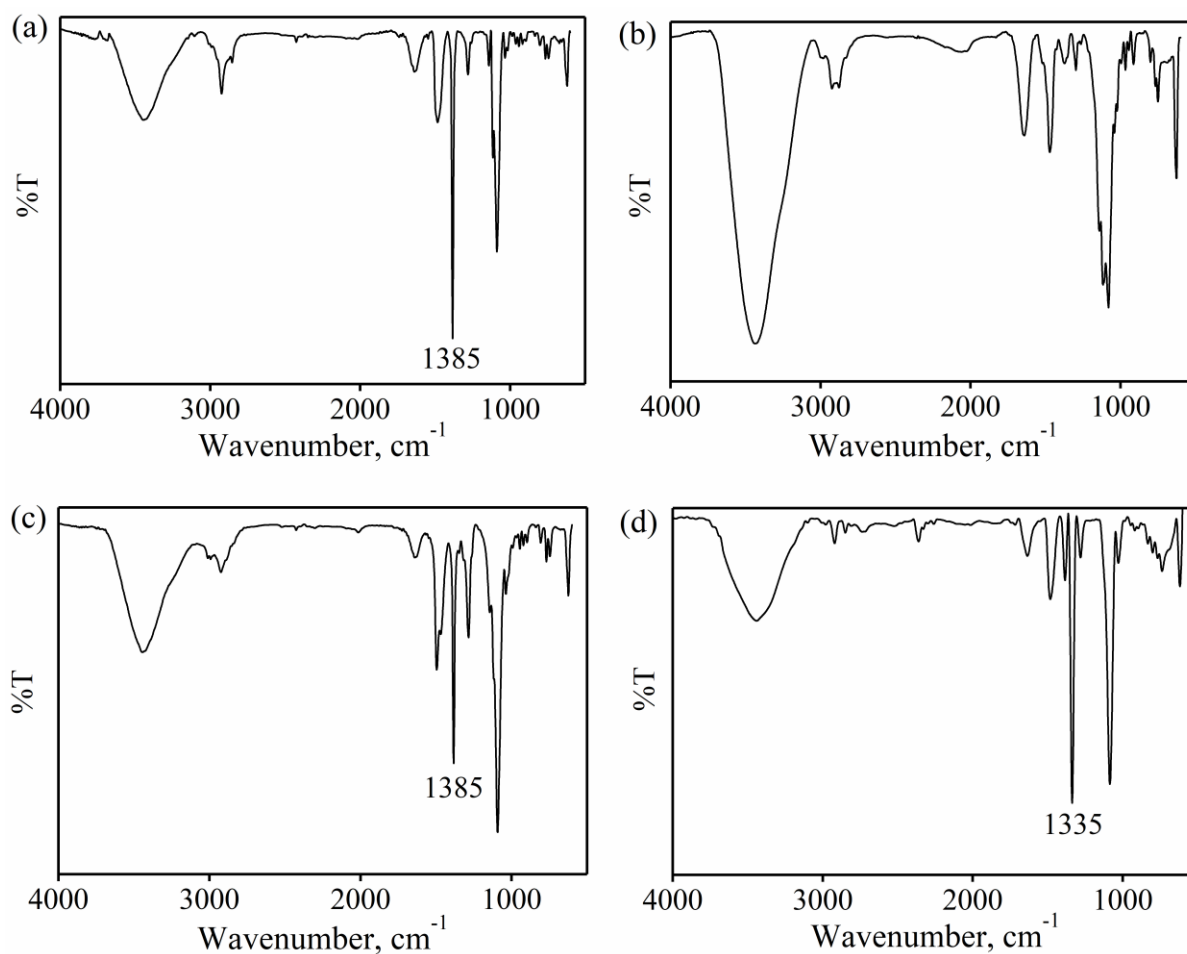
Figure S3. FT-IR spectrum of (a) reaction mixture, ([(12-TMC)Ni^{III}(O$_2$)]$^+$ + NO), recorded after completion of reaction in KBr pellet at 298 K. (b) [(12-TMC)Ni^{III}(O$_2$)]$^+$, recorded in KBr pellet at 298 K (c) ([(12-TMC)Ni^{II}(NO$_3^-$)]$^+$ prepared by reacting [(12TMC)Ni^{II}]$^{2+}$ with NaNO$_3$, in KBr pellet at 298 K. (d) reaction mixture, ([(12-TMC)Ni^{III}(^{18}O$_2$)]$^+$ + NO), recorded after completion of reaction in KBr pellet at 298 K.
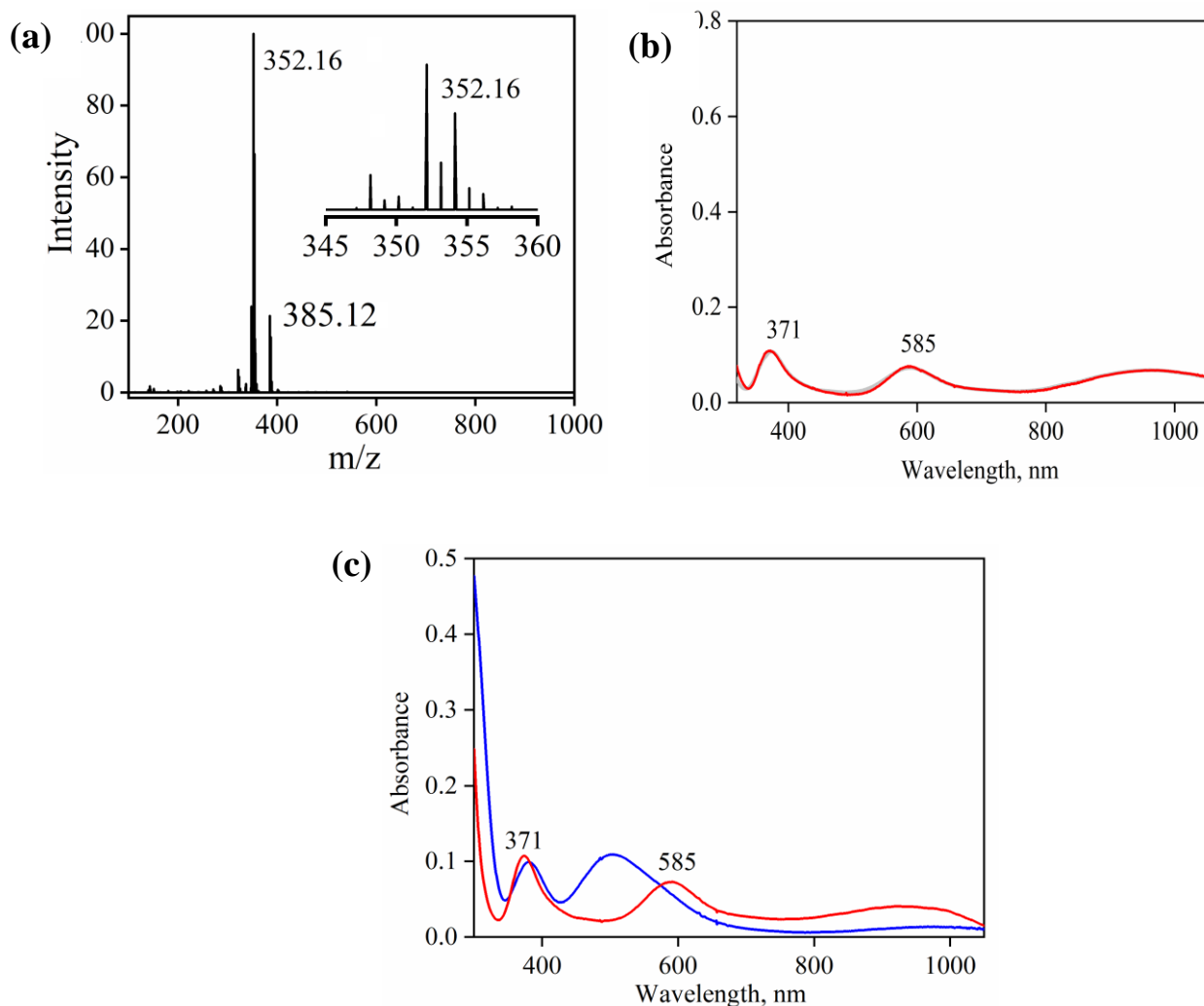
Figure S4. (a) ESI-MS spectrum of **3**, formed in the reaction of ([(12-TMC)Ni^{III}(^{18}O$_2$)]$^+$ + NO, recorded in CH$_3$CN. The peak at *m/z* 352.16 and 385.12 are assigned to be [(12-TMC)Ni^{II}(^{16}ON^{18}O$_2$)]$^+$ (calcd: *m/z* 352.16) and [(12-TMC)Ni^{II}(ClO$_4$)]$^+$ (calcd: *m/z* 385.12), respectively. (b) UV-vis spectra of complex **3** prepare by reacting [(12TMC)Ni^{II}]$^+$ with NaNO$_3$, (0.5mM, grey line) and isolated from the reaction mixture of complex **1** with NO (0.5mM, red line) recorded in CH$_3$CN at 233 K. (c) UV-vis spectra of [(12TMC)Ni^{II}]$^{2+}$, (0.5mM, blue line) and isolated from the reaction mixture of complex **1** with NO (0.5mM, red line) recorded in CH$_3$CN at 233 K.
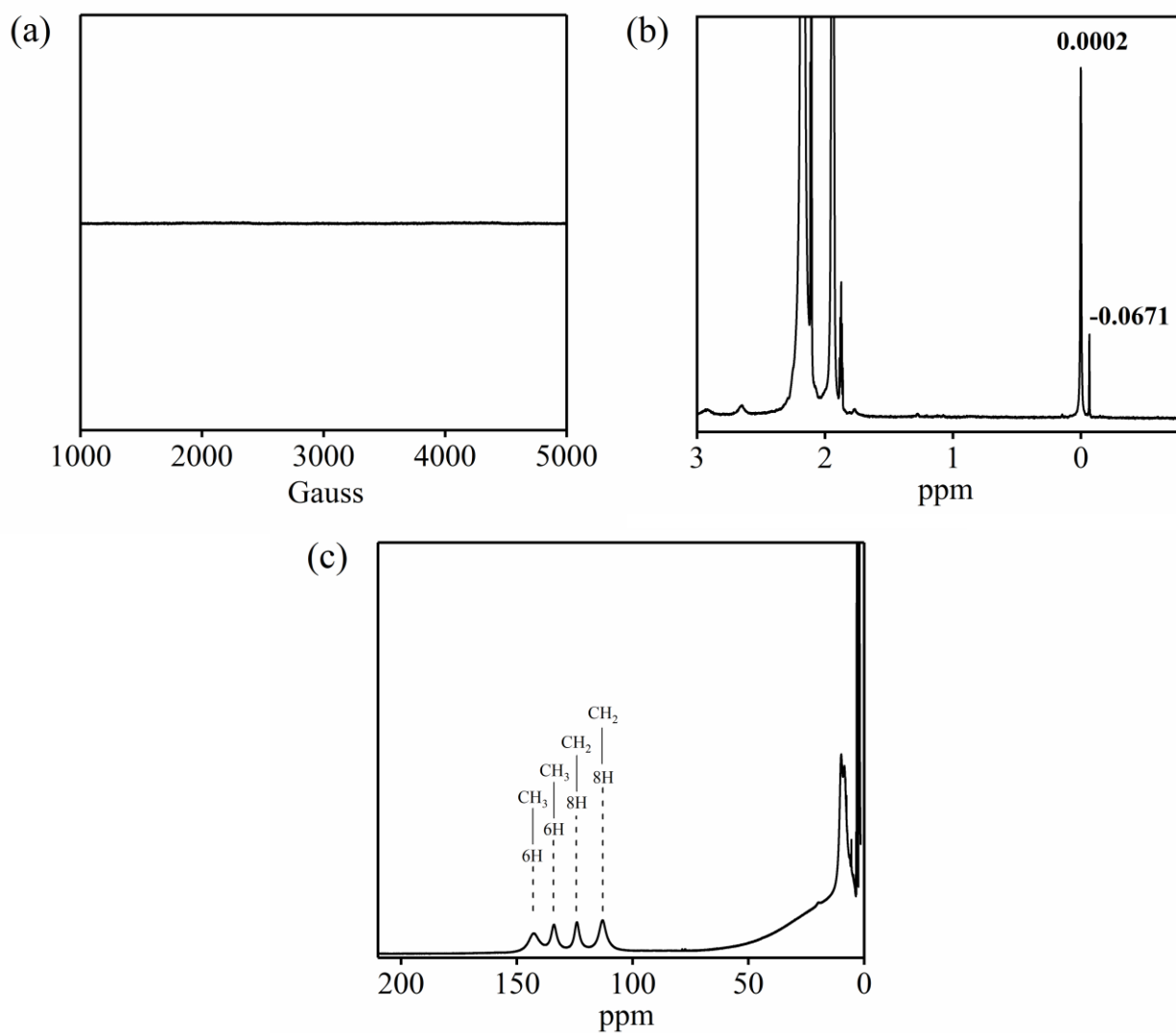
Figure S5. (a) X-band EPR spectrum of **3** (5.0 mM) recorded at 100 K. (b) ^{1}H-NMR (400 MHz) spectra of isolated complex **3** (4 mM) in CD$_3$CN (0.1 % TMS), recorded in a coaxial NMR tube, with inside CD$_3$CN (1.0 % TMS) at RT. (c) Wide range ^{1}H-NMR (400 MHz) spectra of isolated complex **3** (4 mM) in CD$_3$CN.
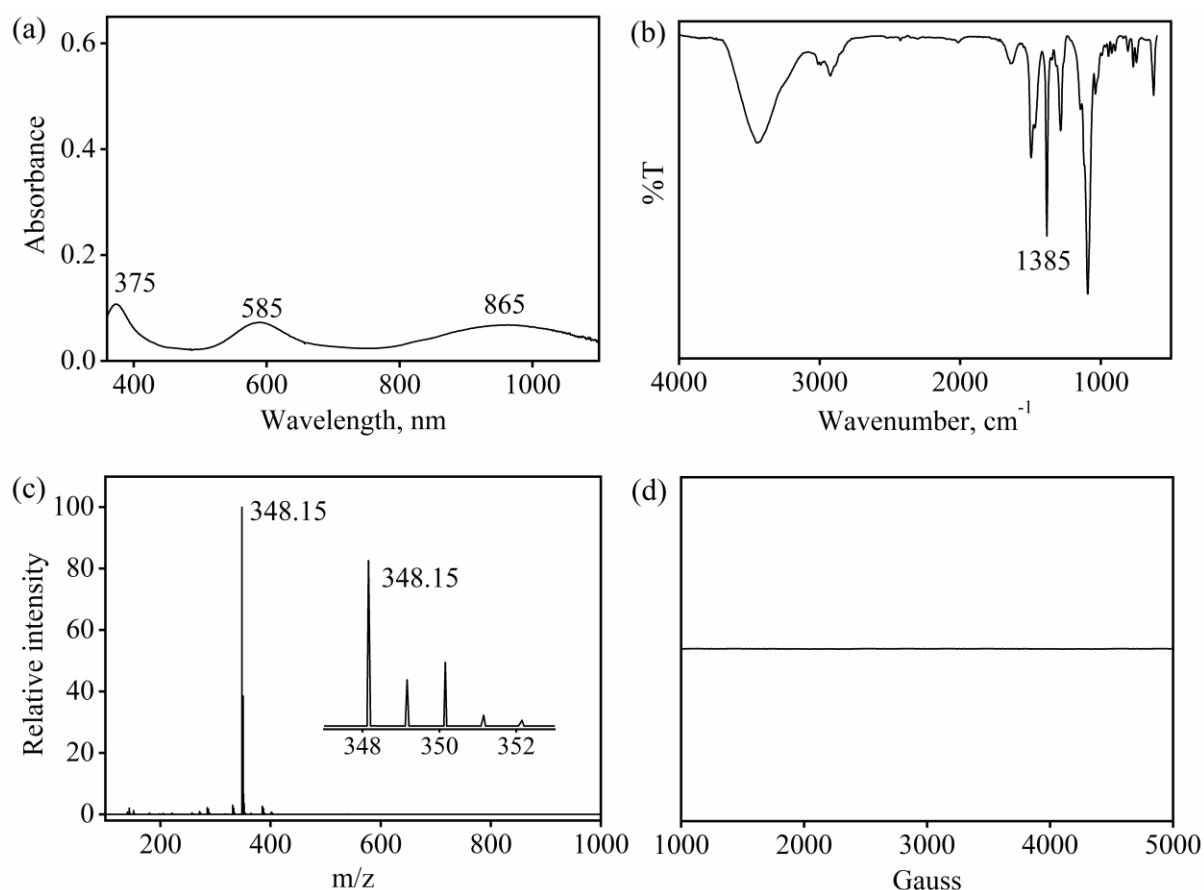
Figure S6. (a) UV-vis spectrum of ([(12-TMC)Ni^{II}(NO$_3^-$)](ClO$_4$) (0.50 mM), prepared by reacting [(12TMC)Ni^{II}]$^+$ with NaNO$_3$, recorded in CH$_3$CN at 233 K. Spectrum shows characteristic absorption band (375 nm, 585 nm and 865 nm) for ([(12-TMC)Ni^{II}(NO$_3^-$)](ClO$_4$). (b) FT-IR spectrum of ([(12-TMC)Ni^{II}(NO$_3^-$)](ClO$_4$) recorded in KBr pellet at 298 K. The spectrum showed the peaks for aliphatic chain (2925 cm^{-1}), Ni^{II}NO$_3^-$ (1385 cm^{-1}), and for ClO$_4^-$ (1100 cm^{-1}). (c) ESI-MS spectrum of ([(12-TMC)Ni^{II}(NO$_3^-$)](ClO$_4$) recorded in CH$_3$CN. The peak at *m/z* 348.15 is assigned to be [(12-TMC)Ni^{II}(NO$_3^-$)]$^+$ (calcd: *m/z* 348.15). (d) X-band EPR spectrum of ([(12-TMC)Ni^{II}(NO$_3^-$)](ClO$_4$) (5.0 mM) recorded at 100 K.
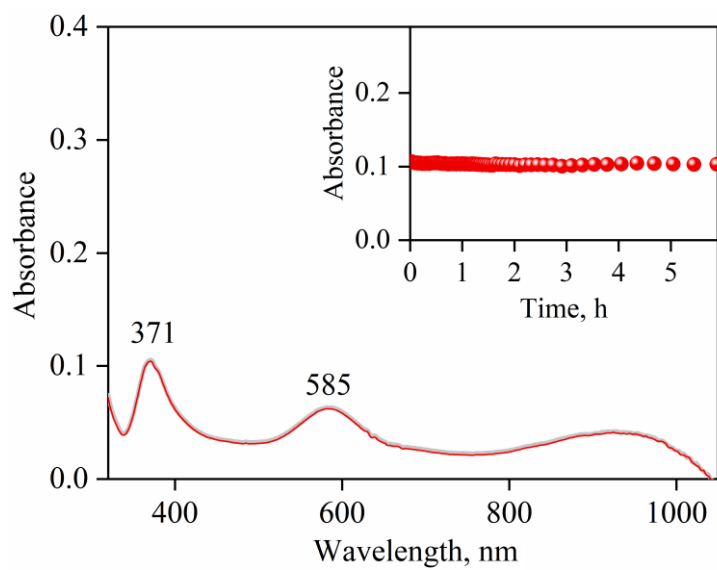
Figure S7. UV-vis spectra of natural decay of complex **3** recorded in CH₃CN at 298 K. The Inset shows the time course of the natural decay of **3** (red circles) monitored at 371 nm.
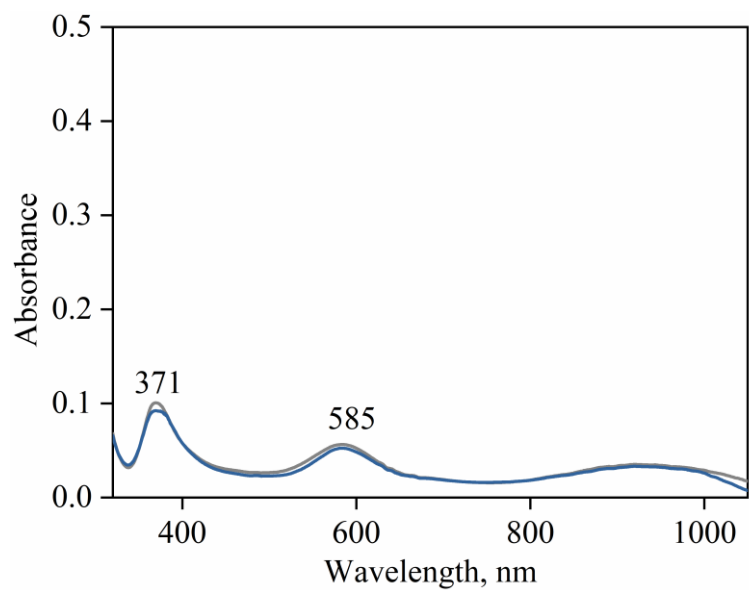
Figure S8. UV-vis spectra of 0.5mM pure isolated complex **3** (grey line) and complex **3** formed in the reaction of 0.5mM of complex **1** with NO (blue line).
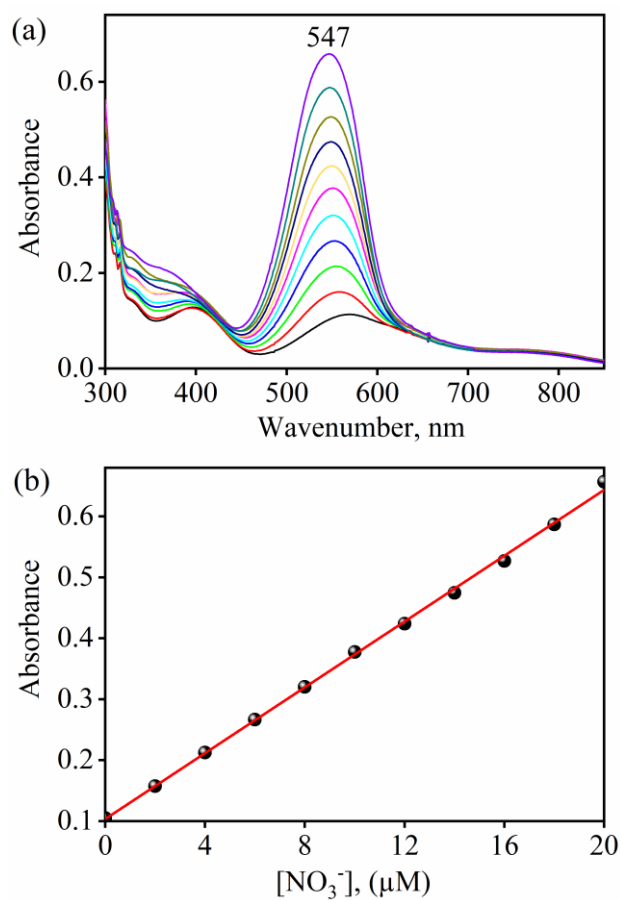
Figure S9. UV-vis spectral changes showing the increase in the absorbance at 547 nm (absorbance band due to the formation of azo dye) by addition of varying amounts of Griess reagent to $NaNO_3$ solutions in various concentrations (0, 2.0, 4.0, 6.0, 8.0, 10, 12, 14, 16, 18, 20 μM) at 298 K. (b) Spectral calibiration curve for the formation of peak at 547 nm as a function of equivalents of $NaNO_3$ in increments of 0, 2.0, 4.0, 6.0, 8.0, 10, 12, 14, 16, 18, 20.
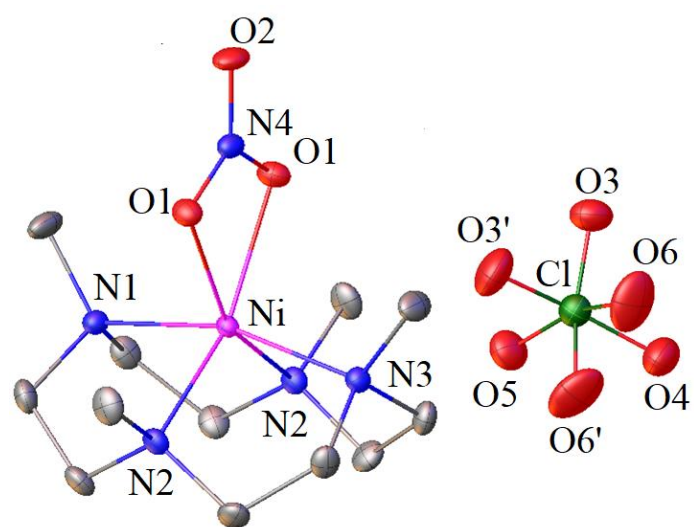
Figure S10. Displacement ellipsoid plots (30 % probability) of [(12-TMC)Ni^{II}(NO$_3$)](ClO$_4$)

(**3**) at 293 K. Disordered portions and the H atoms have been removed for clarity.
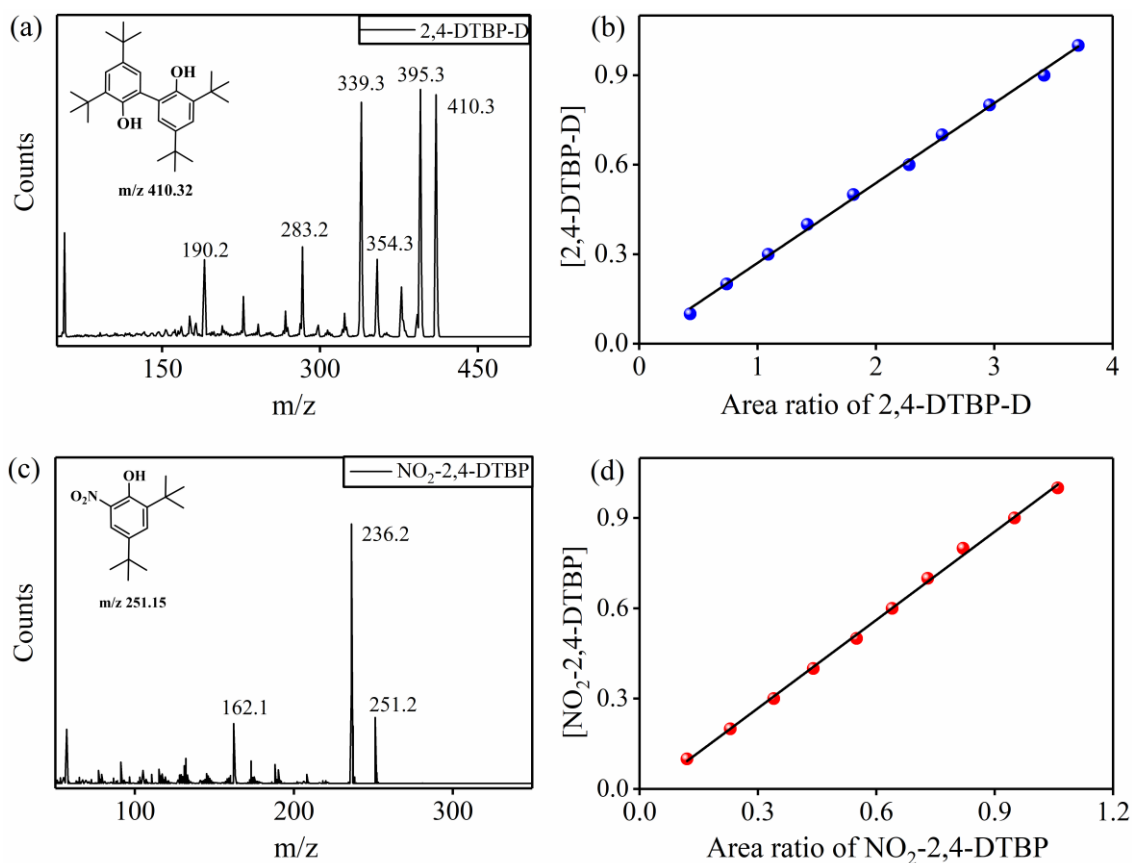
Figure S11. GC-MS characterisation of (a) 2,4-DTBP-dimer (2,4-DTBP-D); The peaks at *m/z* 410.3, 395.3, 339.3 and 190.2 are assigned to be 2,4-DTBP-D, loss of CH_3 from 2,4-DTBP-D, loss of C_4H_8 and CH_3 from 2,4-DTBP-D and loss of CH_3 from monomer 2,4-DTBP (b) Calibration plot for 2,4-DTBP-D. (c) nitro-2,4-DTBP (NO_2-2,4-DTBP): The peaks at *m/z* 251.2 and 236.2 are assigned to be nitro-2,4-DTBP and loss of CH_3 from nitro-2,4-DTBP. (d) Calibration plot for NO_2-2,4-DTBP.The peaks were compared with the NIST standard library.
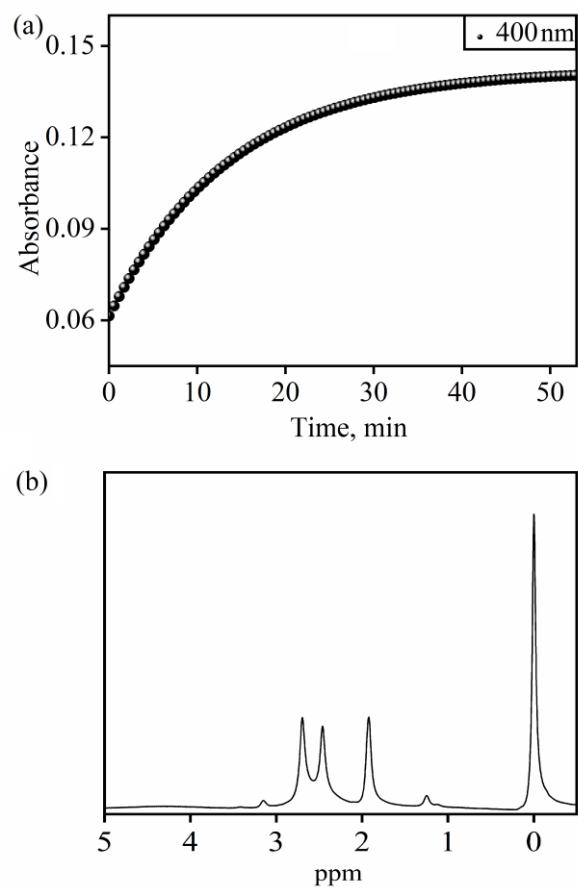
Figure S12. (a) Time course of the reaction of 3 (0.5mM) with 5eqv. H_2O_2 + 2.5eqv. Et_3N monitored at 400 nm in CH_3CN at 233 K. (b)^{1}H-NMR (400 MHz) spectra of product obtained in the reaction of **3** with H_2O_2/TEA in CD_3CN at 298 K.
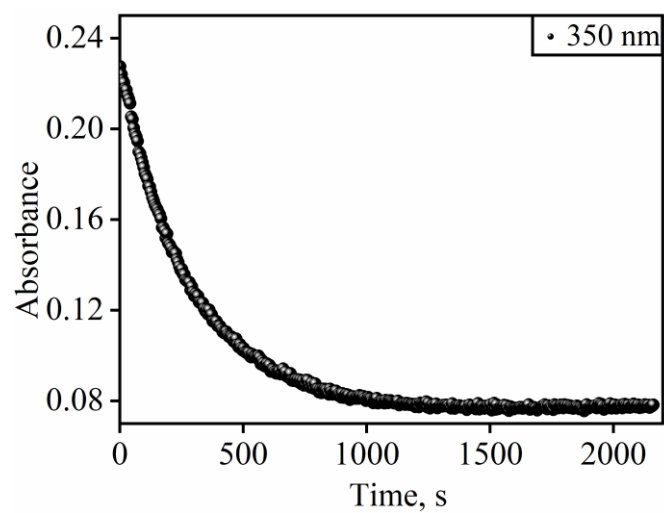
Figure S13. Time course of the reaction of **2** (0.5 mM) with NO monitored at 350 nm in CH$_3$CN at 233 K.
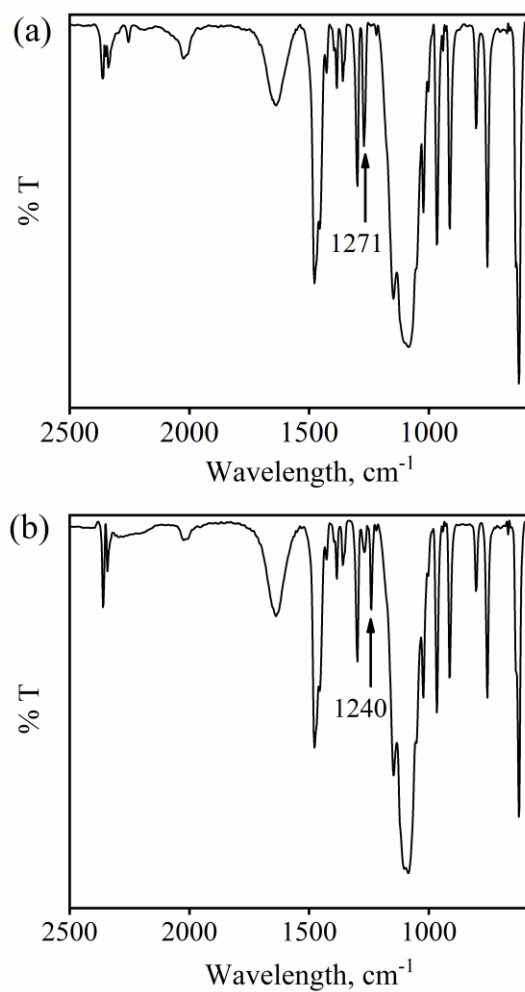
Figure S14. FT-IR spectrum of (a) reaction mixture, ([(12-TMC)Co^{III}(O$_2$)]$^+$ + NO), recorded after completion of reaction in KBr pellet at 298 K. (b) ([(12-TMC)Co^{III}(^{18}O$_2$)]$^+$ + NO), recorded in KBr pellet at 298 K
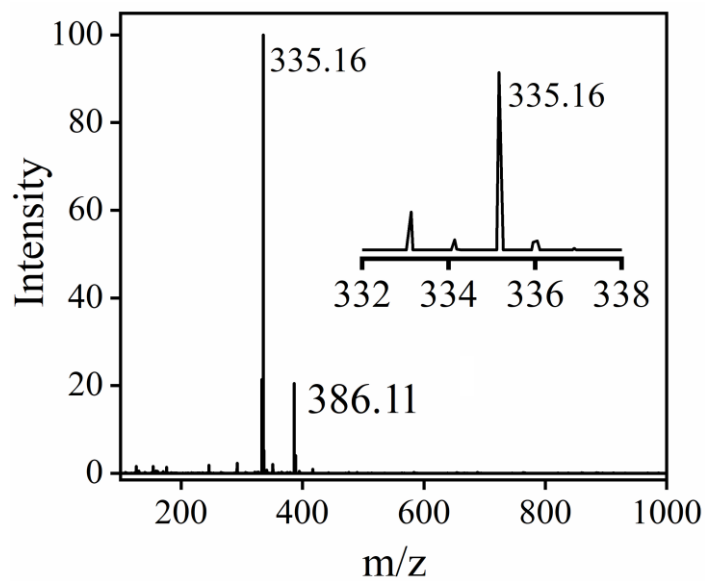
Figure S15. ESI-MS spectrum of **4**, formed in the reaction of $([(12\text{-TMC})Co^{III}(^{18}O_2)]^+ + NO$, recorded in CH_3CN. The peak at *m/z* 335.16 and 386.11 are assigned to be $[(12\text{-}TMC)Co^{II}(^{16}ON^{18}O)]^+$ (calcd: *m/z* 335.16) and $[(12\text{-}TMC)Co^{II}(ClO_4)]^+$ (calcd: *m/z* 386.11), respectively.
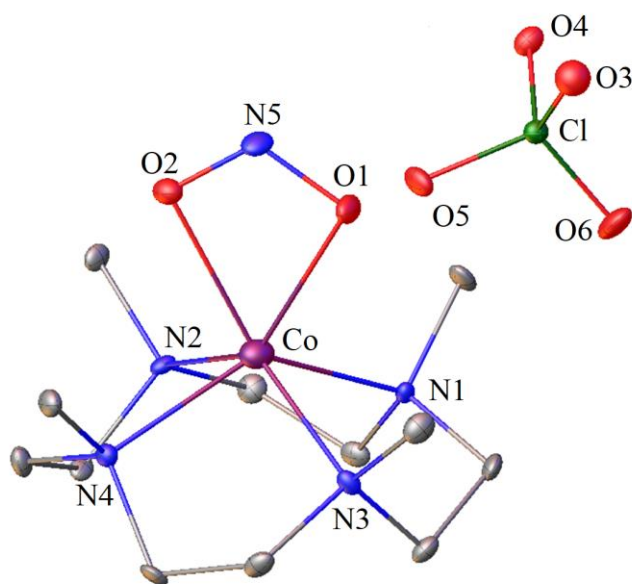
Figure S16. Displacement ellipsoid plots (30 % probability) of [(12-TMC)Co^{II}(NO$_2$)](ClO$_4$) (**4**) at 293 K. Disordered portions and the H atoms have been removed for clarity.
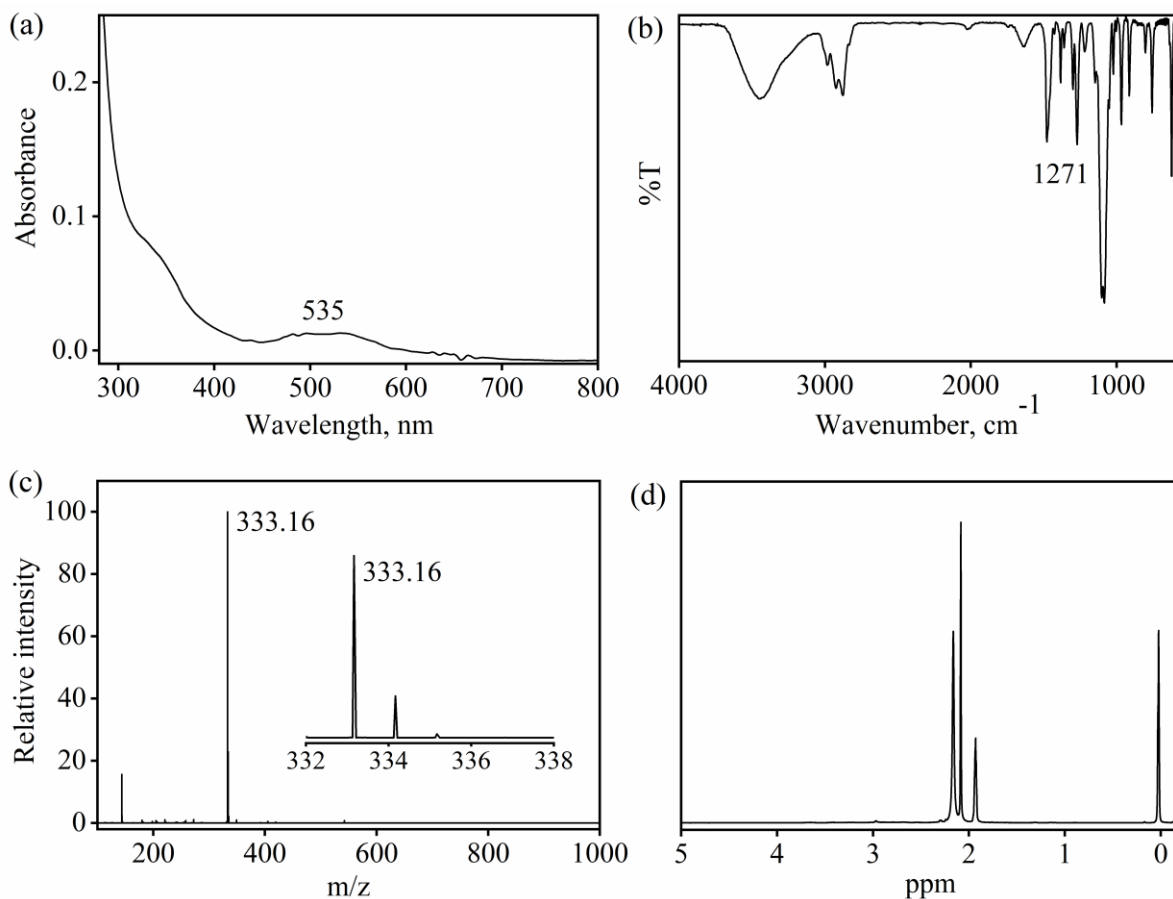
Figure S17. (a) UV-vis spectrum of ([(12-TMC)Co^{II}(NO$_2^-$)](ClO$_4$) (0.50 mM), prepared by reacting [(12TMC)Co^{II}]$^+$ with NaNO$_2$, recorded in CH$_3$CN at 233 K. Spectrum shows the characteristic absorption band at 535 nm for ([(12-TMC)Co^{II}(NO$_2^-$)](ClO$_4$). (b) FT-IR spectrum of ([(12-TMC)Co^{II}(NO$_2^-$)](ClO$_4$) recorded in KBr pellet at 298 K. The spectrum showed the peaks for aliphatic chain (2925 cm^{-1}), Co^{II}NO$_2^-$ (1271 cm^{-1}), and for ClO$_4^-$ (1100 cm^{-1}). (c) ESI-MS spectrum of ([(12-TMC)Co^{II}(NO$_2^-$)](ClO$_4$) recorded in CH$_3$CN. The peaks at *m/z* 333.16 is assigned to be [(12-TMC)Co^{II}(NO$_2^-$)]$^+$ (calcd: *m/z* 333.16). (d) ^{1}H-NMR (400 MHz) spectra of complex ([(12-TMC)Co^{II}(NO$_2^-$)](ClO$_4$) (40 mM) in CD$_3$CN at RT.
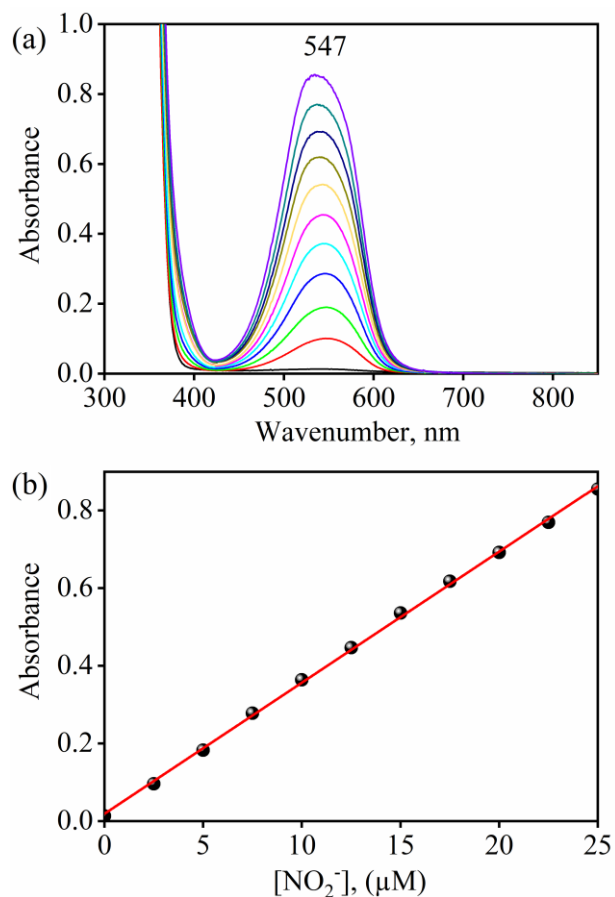
Figure S18. UV-vis spectral changes showing the increase in the absorbance at 547 nm (absorbance band due to the formation of azo dye) by addition of varying amounts of Griess reagent to NaNO$_2$ solutions in various concentrations (0, 2.5, 5.0, 7.5, 10, 12.5, 15, 17.5, 20, 22.5, 25 µM) at 298 K. (b) Spectral calibiration curve for the formation of peak at 547 nm as a function of equivalents of NaNO$_2$ in increments of 0, 2.5, 5.0, 7.5, 10, 12.5, 15, 17.5, 20, 22.5, 25.
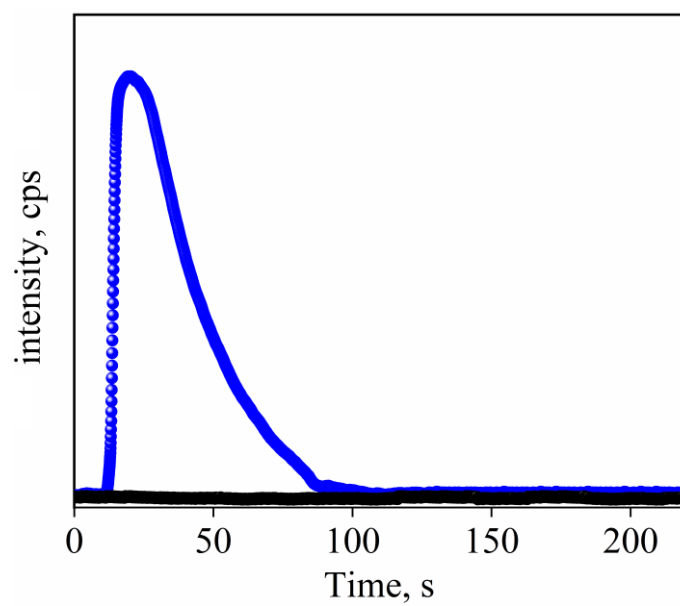
Figure S19. Mass spectra of formation of O_2 in the reaction of complex **2** (5.0 mM) with 1 equivalent of NO.
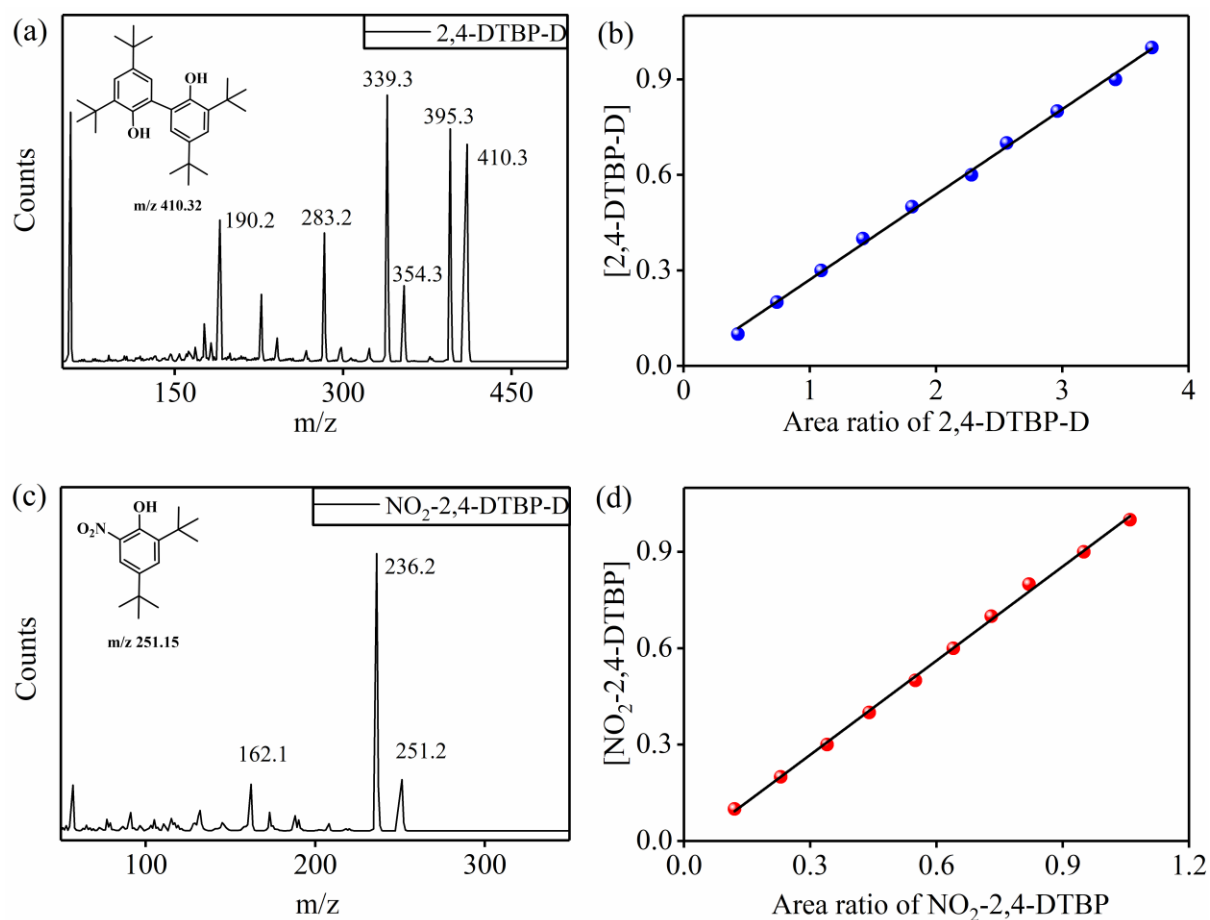
Figure S20. GC-MS characterisation of (a) 2,4-DTBP-D; The peaks at m/z 410.3, 395.3, 354.3, 339.3, 283.2 and 190.2 are assigned to be 2,4-DTBP-D, loss of CH_3 from 2,4-DTBP-D, loss of C_4H_8 and CH_3 from 2,4-DTBP-D and loss of CH_3 from monomer 2,4-DTBP (b) Calibration plot for 2,4-DTBP-D. (c) nitro-2,4-DTBP: The peaks at m/z 251.2, 162.1 and 236.2 are assigned to be nitro-2,4-DTBP and loss of CH_3 from nitro-2,4-DTBP. (d) Calibration plot for nitro-2,4-DTBP. The peaks were compared with the NIST standard library.
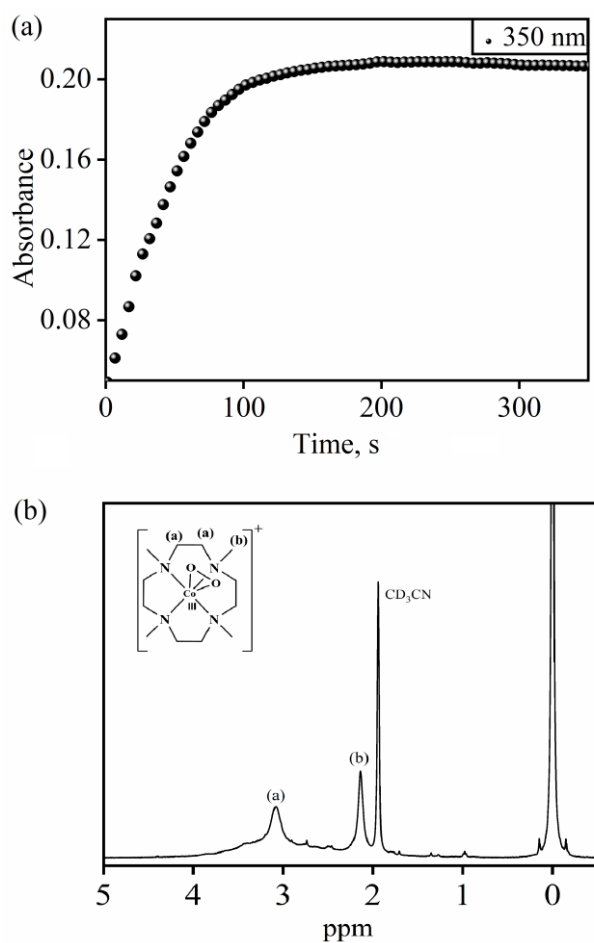
Figure S21. (a) Time course of the reaction of **4** (0.5mM) with 5eqv. H_2O_2 + 2.5eqv. Et_3N monitored at 350 nm in CH_3CN at 233 K. (b)^{1}H-NMR (400 MHz) spectra of product obtained in the reaction of **4** with H_2O_2/TEA in CD_3CN at 298 K.
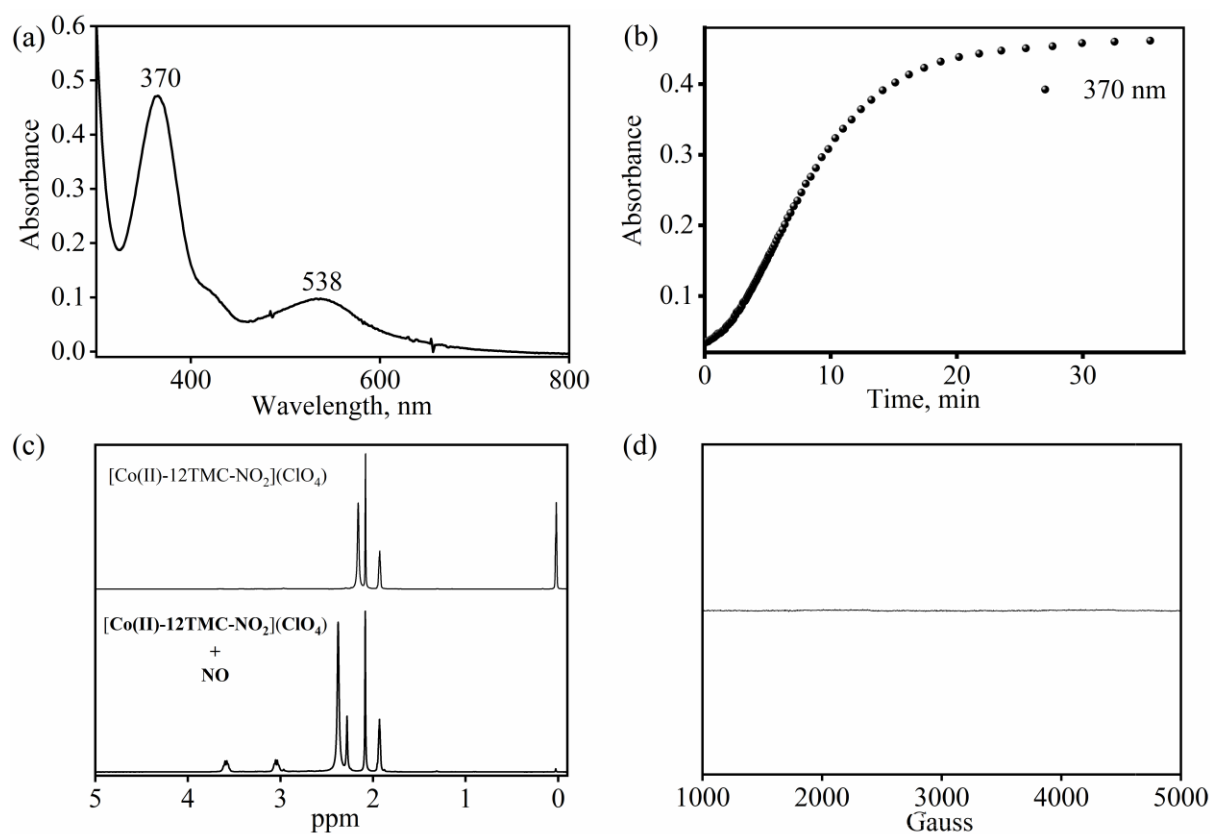
Figure S22. (a) UV-vis spectrum of complex **4** (0.50 mM),+ excess NO recorded in CH$_3$CN at 233 K. Spectrum shows the characteristic absorption band at 370 nm for [(12-TMC)Co^{II}(NO)]$^{2+}$. (b) Time course of the reaction of **4** (0.5 mM) with excess NO monitored at 370 nm in CH$_3$CN at 233 K. (c) ^{1}H NMR spectra of complex **4** and after the reaction of complex **4** + excess NO recorded in CD$_3$CN at RT. (d) X-band EPR spectrum of isolated product of complex **4** + excess NO recorded at 100 K.
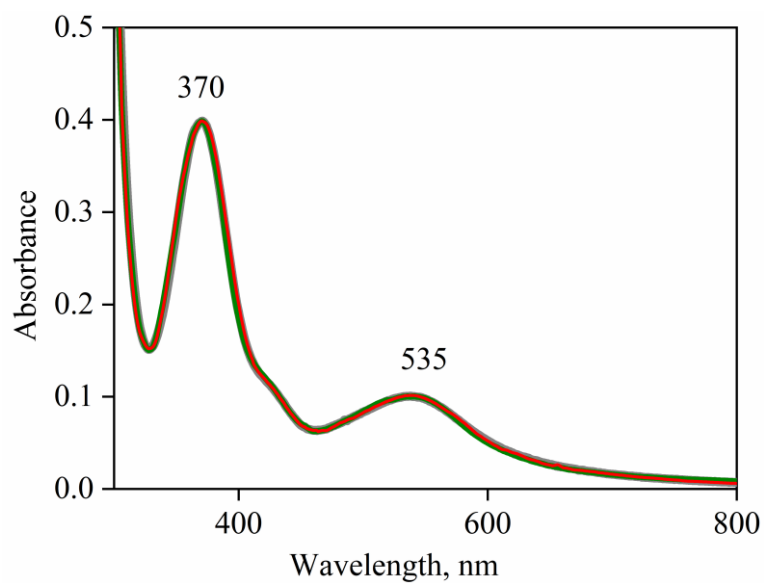
Figure S23. UV-vis spectra of 0.5mM complex **5** with different anions. [(12-TMC)Co^{II}(NO)](ClO$_4$)$_2$ (grey line), [(12-TMC)Co^{II}(NO)](BF$_4$)$_2$ (green line), [(12-TMC)Co^{II}(NO)](BPh$_4$)$_2$ (red line).
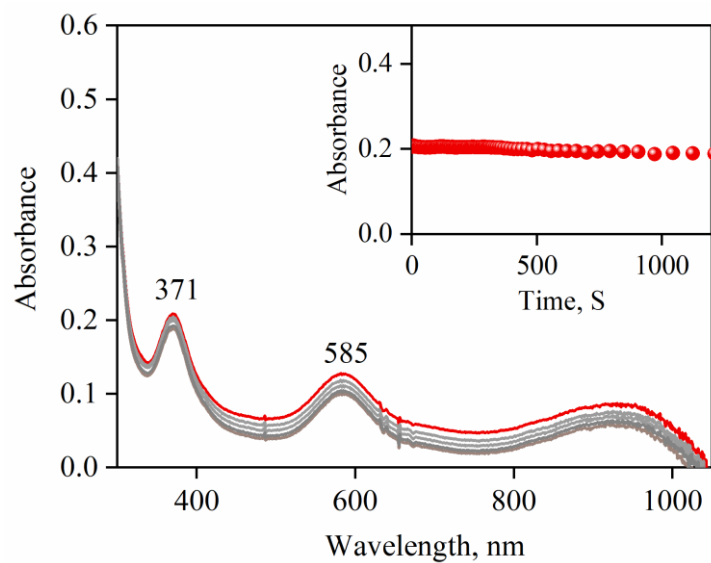
Figure S24. UV-vis spectra for the complex **3** with NO. The Inset shows the time course of the natural decay of **3** (red circles) monitored at 371 nm in CH$_3$CN at 233 K.